

Modulating the Coordination Environment of Lithium Bonds for High Performance Polymer Electrolyte Batteries

Zhilong Tian,[#] Lei Hou,[#] Doudou Feng, Yucong Jiao,* and Peiyi Wu*



Cite This: *ACS Nano* 2023, 17, 3786–3796



Read Online

ACCESS |

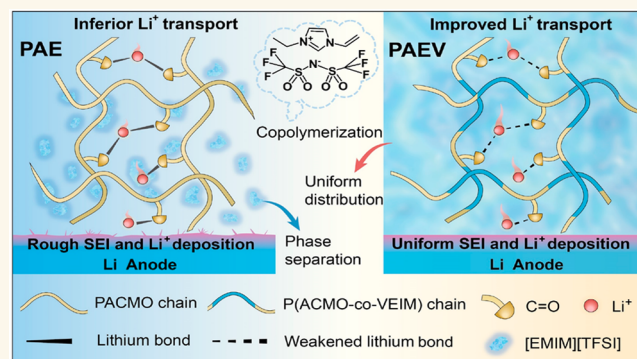
Metrics & More

Article Recommendations

Supporting Information

ABSTRACT: The new-generation lithium metal batteries require polymer electrolytes with high ionic conductivity and mechanical properties. However, the performance of the polymer electrolytes is severely influenced by the lithium bond formation between the functional groups and lithium ions (Li^+), which has barely been considered in the past. Herein, a lithium bond enriched polymer gel (PAEV) is elaborately designed by copolymerizing 4-acryloylmorpholine (ACMO) and 1-vinyl-3-ethyl imidazolium bis(trifluoromethylsulfonyl)-imide ([VEIM][TFSI]) in 1-ethyl-3-methyl imidazolium bis(trifluoromethylsulfonyl)imide ([EMIM][TFSI]) with the presence of LiFSI. The lithium bonds formed between LiFSI and carbonyl groups in PACMO can be regulated by the Li^+ coordination number, and further weakened by the hydrogen bonds with [EMIM][TFSI] and poly[VEIM][TFSI], to effectively render the polymer electrolyte with adjustable ionic conductivity and tunable mechanical property. In addition, with the regulated coordination environment of Li^+ , the LiF and Li_3N layer can be uniformly formed on the Li surface to facilitate Li^+ nucleation and deposition. As a consequence, the PAEV electrolyte confers the Li/LiFePO₄ (LFP) battery with high capacity of 124 mA h g⁻¹ at 1 C under 25 °C, and 152 mA h g⁻¹ under 50 °C. This work can promote the development of high performance polymer electrolyte via lithium bond manipulation.

KEYWORDS: lithium bond, Li^+ coordination number, polymer electrolyte, mechanical property, ionic conductivity



Lithium metal batteries have been recognized as the next generation of batteries with high energy densities, due to the high theoretical capacity (3860 mA h g⁻¹) and low electrochemical potential of lithium.¹ Before commercialization, the safety issues triggered by the lithium dendrite formation and the flammable organic electrolyte should be thoroughly resolved. Polymer electrolytes have drawn great attention as potential solutions for the above-mentioned issues, ascribed to their intrinsic organic-electrolyte-free feature, no flammability, easy processing, and high interfacial adaptivity.^{2–5}

Plenty kinds of polymer electrolyte have been designed to endow the lithium battery with high performance, including poly(ethylene oxide) (PEO),^{6,7} polysiloxane (PS)^{8,9} and polycarbonate (PC)^{10–12} based electrolytes, which all exhibit great potentials recently. However, these electrolytes still confront challenges: the ionic conductivity of the PEO-based electrolyte is relatively lower, the mechanical strength and interfacial compatibility of the PS-based electrolyte are inferior, and the electrochemical stability at high voltage and

mechanical properties of the PC-based electrolyte are deficient for large-scale production.¹³ Thereby, engineering a polymer gel electrolyte with high ionic conductivity and lithium transference number, excellent mechanical strength, and great electrochemical stability in a wide voltage range remains a great challenge. Recently, employing a high concentration of salts, ionic liquids or poly(ionic liquids) has been demonstrated to be effective for improving the ionic conductivity and lithium transference number of the solid polymer batteries, but the mechanical strength and the electrochemical performance of these polymer electrolytes still need to be significantly optimized especially at room temperature.^{14,15}

Received: November 24, 2022

Accepted: February 2, 2023

Published: February 6, 2023



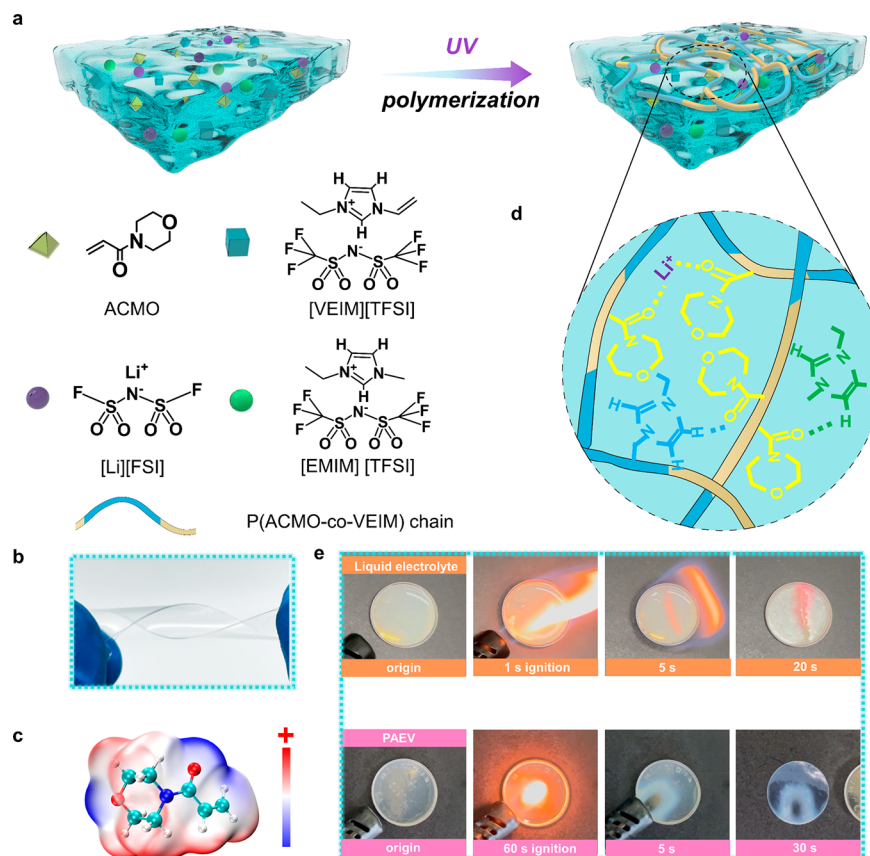


Figure 1. Schematic illustrations and the characterizations of the PAEV polymer electrolyte. (a) Molecular structures of PAEV precursors. (b) Digital photos of the PAEV. (c) The surface electrostatic potential of ACMO. (d) Illustrations for the interactions in PAEV. (e) Flammability tests for liquid electrolyte and PAEV. The 60 s ignition means burning the electrolyte for 60 s. 5 s and 30 s are the images of the electrolyte after stopping burning with lighter for 5 and 30 s, respectively.

In past decades, lithium bonds have been considered as the analogous interactions to hydrogen bonds.^{16–18} Nonetheless, due to the metallic nature and large radius of lithium, the lithium bonds can coordinate with more than one functional group of the polymer chains, resulting in enhanced mechanical strength when formed in the polymer gel. In addition, lithium bonds own no saturation and directionality.¹⁹ With the different ratio of Li⁺ to functional groups, the coordination environment can be regulated; thus, the mechanical property and ionic conductivity can be manipulated in the polymer gel. Furthermore, with an optimized coordination environment, the lithium transfer barrier in lithium bonds is also smaller than hydrogen in hydrogen bonds, which enables the polymer gel with high ionic conductivity in a certain lithium bond density.¹⁹ Recent research has reported that the mechanical property and ionic conductivity can be simultaneously improved with the increase of the lithium salt contents in a 2-methoxyethyl acrylate based polymer.²⁰ Nevertheless, the corresponding coordination models of the lithium salt in polymer with various ratios are still vague, and the relationships of the lithium coordination structure with ionic conductivity and mechanical property still need to be scrutinized.

In this work, we employ the carbonyl abundant monomer 4-acryloylmorpholine (ACMO) and imidazole based ionic liquid to engineer an ionic polymer gel electrolyte (PAEV) with Li bis(fluorosulfonyl)imide (LiFSI). The large amounts of carbonyl groups in PACMO can form strong lithium bonds

with LiFSI, which can be dedicated to the mechanical property regulation. In addition, by adjusting the molar ratio of LiFSI and ACMO, the coordination number of Li⁺ can be manipulated, resulting in the optimized mechanical property, ionic conductivity, and lithium transference number. Furthermore, the imidazole groups in [VEIM][TFSI] could compete with the lithium salts to form hydrogen bonds with the carbonyl group of PACMO, and the TFSI⁻ of [VEIM][TFSI] can cocomordinate with Li⁺ and the carbonyl group. Thereby, the transfer barrier of Li⁺ is weakened, leading to higher ionic conductivity and lithium transference number of the gel electrolyte. As a consequence, we demonstrate that the polymer electrolyte can synchronously provide high ionic conductivity and excellent mechanical property at the coordination number around 3 (one Li⁺ to around three carbonyl groups). When employed in lithium metal batteries, the PAEV electrolyte can enhance the battery with a dendrite free performance for 1200 h at 0.3 mA cm⁻², and enable the LiFePO₄ battery with a high cycling performance both at room temperature and 50 °C.

RESULTS AND DISCUSSION

Electrolyte Preparation and Characterization. The schematic illustrations for the fabrication of PAEV and the molecular structures of ACMO, [VEIM][TFSI], [EMIM][TFSI] and LiFSI are shown in Figure 1a. The structure of [VEIM][TFSI] was characterized by FTIR spectra. Compared with [EMIM][TFSI], a double bond can be observed as shown

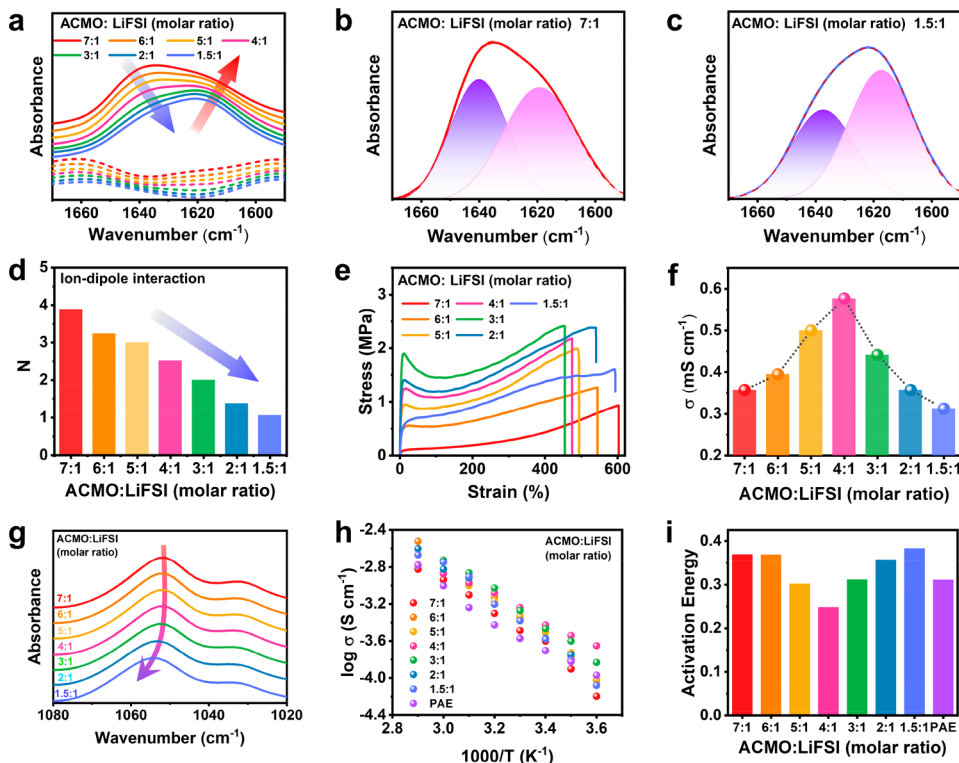


Figure 2. Properties regulation mechanism of the polymer electrolyte. (a) FTIR spectra and the correspond 2nd derivative of the PAEV solid polymer electrolyte with different LiFSI content in the range between 1670 and 1590 cm⁻¹ (dotted lines: 2nd derivative curves). The fitted FTIR spectra of (b) 7:1 and (c) 1.5:1. (d) Number of carbonyls coordinated with Li⁺. (e) Tensile stress–strain curves, (f) ionic conductivity, (g) FTIR range in 1080 to 1020 cm⁻¹, (h) ionic conductivity at different temperatures, (i) activation energy of PAEV polymer electrolyte with different salt concentrations, the mole ratios between ACMO and LiFSI are 7:1, 6:1, 5:1, 4:1, 3:1, 2:1, 1.5:1, respectively.

in Figure S1. The as-polymerized PAEV is transparent and has an excellent mechanical flexibility (Figure 1b). The FTIR spectra were then employed to characterize the structure and molecular interactions of the electrolyte. As exhibited in Figure S2, the characteristic band of the C=C bonds in ACMO (1610 cm⁻¹) and [VEIM][TFSI] (1650 cm⁻¹) disappeared after polymerization, demonstrating the successful polymerization of ACMO and [VEIM][TFSI]. Notably, in Figure S3, the characteristic band of the carbonyl stretching vibration related to PACMO in the PAEV red-shifts from 1638 to 1618 cm⁻¹ with the incorporation of LiFSI, illustrating the lithium bonds formation between Li⁺ and carbonyl groups on PACMO.²¹ The surface electrostatic potential (ESP) of ACMO is shown in Figure 1c. The functional groups of carbonyl in ACMO render more negative ESP values, in consistent with the FTIR results. This can be attributed to the steric hindrance, which makes Li⁺ interact with oxygen atom of carbonyl rather than the oxygen atom of ether on morpholine ring.^{22,23} Besides, both [EMIM][TFSI] and [VEIM][TFSI] can form hydrogen bonds with PACMO,^{24,25} which can alleviate the lithium bonds interaction, and further improve the Li⁺ transport in the PAEV. As shown in Figure S4, the carbonyl groups of pure PACMO own an obvious peak at 1644 cm⁻¹, which can be considered as the dipole–dipole interaction between carbonyl groups. After adding [EMIM][TFSI] to PACMO, the dipole–dipole interactions of the carbonyl groups in PACMO are broken and hydrogen bonds between imidazole and C=O are formed, leading to the red-shift of $\nu(C=O)$ to ~ 1638 cm⁻¹. After further addition of LiFSI, Li⁺ and carbonyl groups form lithium bonds, resulting in the appearance of peak at 1618 cm⁻¹. The strong lithium bonds

may hinder the Li⁺ transport in the polymer electrolyte during battery cycling,^{19,26} and the presence of the hydrogen bonds between ionic liquid and carbonyl groups can weak the lithium bonds and improve the transport of Li⁺. The corresponding schematic diagrams of the interactions in the polymer network are illustrated in Figure 1d. The thermal stability of the PAEV electrolyte is also analyzed. As shown in Figure 1e and Movie S1, the PP separator with liquid electrolyte burns out quickly within one second. In contrast, the PAEV showed excellent nonflammability under the 60 s ignition. This excellent thermal stability of PAEV can ensure the safety of the lithium metal battery.

The lithium bonds coordination or cross-linking behaviors of Li⁺ with PACMO were characterized with FTIR spectra. In Figure 2a, with the molar ratio of LiFSI increasing, the band at 1641 cm⁻¹ presented an intensity decreasing while the band intensity at 1618 cm⁻¹ increased, demonstrating that more carbonyl groups are involved into the lithium bonds formation. According to the second-order derivative spectra, the bands in the range between 1670 and 1590 cm⁻¹ were curve-fitted and calculated with Gaussian curves, as shown in Figure 2b,c and Figure S5. The proportion of the area of 1618 cm⁻¹ band to the total area was counted and depicted in Figure S6. Combined with the different molar ratios of ACMO and LiFSI, the coordination number between Li⁺ and carbonyl group at different molar concentrations can be calculated (Figure 2d). With the increase of LiFSI content, the number of carbonyls coordinated with Li⁺ gradually decreased from 4 to 1. Herein, with multiple lithium bonds for one Li⁺, the Li⁺ can act as a cross-linker in the polymer electrolyte, which severely influences the mechanical property and ionic conductivity.

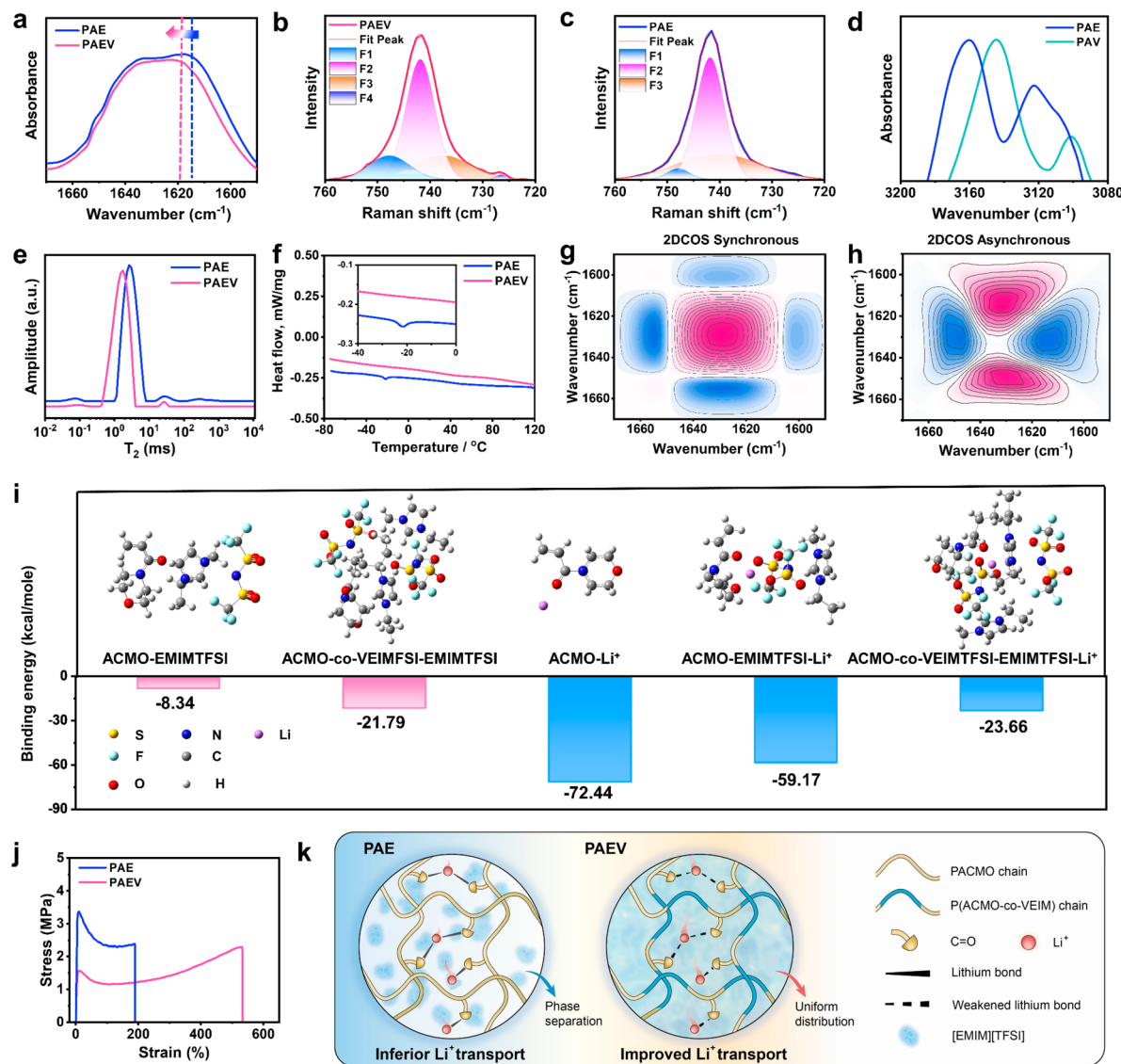


Figure 3. Interaction characterizations of the electrolyte after copolymerizing [VEIM][TFSI]. (a) FTIR spectra of the PAE and PAEV in the range between 1680–1580 cm⁻¹. Raman spectra of (b) PAEV and (c) PAE and the corresponding fitting curves. (d) FTIR spectra of PAE and PAV in the range of 3200–3080 cm⁻¹. (e) LF-NMR and (f) DSC curves of PAE and PAEV. 2DCOS (g) synchronous and (h) asynchronous spectra. The warm colors (pink) represent positive intensities, while cold colors (blue) represent negative intensities. (i) Density functional theory (DFT) calculations. (j) Tensile stress–strain curves of PAE and PAEV. (k) Schematic diagrams of Li⁺ transport modes in PAE and PAEV.

With the increasing of LiFSI from 7:1 to 3:1 (ACMO: LiFSI), the elongation of PAEV decreased and the stress at break increased, on account of more lithium bonds' formation. Interestingly, with the molar ratio of LiFSI increased to 1.5:1 (ACMO: LiFSI), the elongation increased and the stress at break decreased. This can be attributed to the specific characteristics of lithium bonds. The metallic property enables that the Li⁺ can coordinate or cross-link with more than one functional group. When the molar ratio of LiFSI lowering than 3:1 (ACMO: LiFSI), the coordination number is greater than 2 (Figure 2d), demonstrating that Li⁺ acts as the cross-linker. When the molar ratio of LiFSI increased (2:1 and 1.5:1 for ACMO: LiFSI), the coordination number is lower than 2 and the effect of cross-linking role of Li⁺ is suppressed, thus leading to the decrease of the mechanical strength and increase of breaking strain (Figure 2e). The ionic conductivity is also influenced by the coordination number. As shown in Figure 2f,

with the LiFSI concentration rising, the ionic conductivity increases due to more Li⁺ transport in the polymer electrolyte. At the same time, the coordinate number of the Li⁺ is also decreasing. It should be noted that the high coordination number will deteriorate the migration of Li⁺ due to the stronger interactions with Li⁺.²⁷ When the molar ratio of ACMO to LiFSI reaches 4:1, the coordination number is near 3 (each Li⁺ is coordinated with 3 carbonyls on average), and the polymer electrolyte can deliver a high ionic conductivity of 0.57 mS cm⁻¹. The interactions were then characterized by FTIR spectra. As Figure 2g shows, the band at 1050 cm⁻¹ can be assigned to the antisymmetric bending of the –SNS– groups in the TFSI anions for [EMIM][TFSI].²⁸ When the molar ratio of LiFSI exceeds 3:1 of ACMO to LiFSI, the peak shifts obviously to higher wavenumber, illustrating that more TFSI⁻ anions coordinate with Li⁺, and the interaction between Li⁺ and C=O is weakened. This result is also verified by

Raman spectroscopy. As exhibited in **Figure S7**, with the ratio exceeding 3:1 for ACMO to LiFSI, the peak at around 742 cm⁻¹ shifts to higher frequency due to the formation of Li⁺-xTFSI⁻ complex.^{29,30} The ionic conductivity may decrease when too many TFSI⁻ anions coordinate with one Li⁺.^{15,31} The ionic conductivities of the samples with different LiFSI contents are evaluated at different temperature, where the ionic conductivities of all the electrolytes fit well with the Vogel-Tamman-Fulcher (VTF) empirical eq (**Figure 2h**). The activation energies of the electrolytes are then estimated in **Figure 2i**. Compared to other electrolytes, the electrolyte with the molar ratio of 4:1 for ACMO to LiFSI renders the lowest activation energy, attributed to its more appropriate coordination number for Li⁺ transport. Considering both effects of LiFSI content on the mechanical performance and ionic conductivity of the electrolytes, we choose the molar ratio of ACMO to lithium salt of 4:1 as an optimum for further study.

Apart from the lithium bonds, hydrogen bonds exist between the imidazole groups of ionic liquids and the carbonyl groups of PACMO in the electrolyte system. For better demonstration, the polymer electrolyte containing PACMO, [EMIM][TFSI] and LiFSI was prepared and denoted as PAE. Low-field nuclear magnetic resonance (LF-NMR) was employed to characterize the hydrogen bonding interactions with regard to the ionic liquids. The relaxation time (T_2) represents the binding degree of hydrogen in [EMIM][TFSI], reflecting the strength of hydrogen bonds. As shown in **Figure S8**, pure [EMIM][TFSI] shows T_2 in 100–1000 ms, which could be related to the free state of H atom on imidazole ring. For the polymer gel without LiFSI, the peak shifts to around 0.1–1 ms, indicating the strong hydrogen bonding interactions between [EMIM][TFSI] and polymer chains. With the existence of LiFSI, the relaxation time of T_2 increases, illustrating that the formation of lithium bonds between Li⁺ and carbonyl groups can influence the hydrogen bond between [EMIM][TFSI] and carbonyl groups.

The impact of the polymerizable ionic liquids ([VEIM]-[TFSI]) (PIL) on the lithium bonds regulation was then evaluated. Herein, it is notable that the addition of a certain amount of LiFSI would make the PACMO/[EMIM][TFSI] gel opaque (**Figure S9**), indicating the aggregation of ionic liquids caused by the weakening of hydrogen bonding between PACMO and [EMIM][TFSI] with the presence of LiFSI. The nonuniform and nonideal state in the PAE electrolyte are not conducive to the rapid conduction of Li⁺. In contrast, the PIL can keep the PAEV electrolyte smooth and transparent with no obvious phase separation, illustrating the uniform distribution of ionic liquid in the electrolyte for improved Li⁺ transport in the electrolyte, due to the proper lithium bonds regulation in PAEV.

FTIR spectra were then employed to elucidate the effect of PIL segments on the molecular interactions in the electrolytes. As shown in **Figure 3a**, after copolymerizing [VEIM][TFSI] in the polymer chains, the peak related to the carbonyl groups bonded with Li⁺ shifts to a higher wavenumber and the fraction of the peak is reduced, revealing that lithium bond between Li⁺ and carbonyl is weakened in the PAEV. The ions coordination environment in PAE and PAEV products was further studied by Raman spectroscopy (**Figure 3b**). The strong peak at around 747 cm⁻¹ (F1) corresponds to Li⁺-xTFSI⁻ coordination structure, 741 cm⁻¹ (F2) is attributed to the free TFSI⁻, and the peaks at around 737 (F3) and 727 cm⁻¹ (F4) are related to the FSI⁻ and free FSI⁻

respectively.³² Compared to TFSI⁻ peak in the PAE product, the peak area of F1 in the PAEV product is significantly increased, illustrating that the percentage of bound TFSI⁻ in PAEV product is higher than that in PAE. Since the coordination between FSI⁻ and Li⁺ is slightly stronger than that of TFSI⁻, the solvent environment of Li⁺ is analyzed by the content of bound TFSI⁻ in this system.

The Li coordination number (χ) is then calculated and listed in **Table S1**. As shown, the coordination number of Li⁺ to TFSI⁻ in PAE is 0.2 (one Li⁺ with 0.2 TFSI⁻), verifying that only small amounts of TFSI⁻ participate in the Li⁺ transport. Thereby, the Li⁺ mainly transfers along the oxygen atoms of PACMO in PAE electrolyte. In contrast, with the addition of PIL, the coordination number of Li⁺ to TFSI⁻ increased to 0.8. At this coordination number, the TFSI⁻ of PIL can act as a bridge to improve the Li⁺ transport by cocrordination, resulting in the enhanced Li⁺ diffusion.^{33,34}

For further illustration, a PAV electrolyte was prepared by replacing the ionic liquids in PAE with PIL of the same molar. As the FTIR spectra in **Figure 3d** show, the C–H stretching vibration for the imidazole groups of PIL in PAV shifts significantly compared to PAE, verifying the strong hydrogen bonds formation between imidazole of PIL with carbonyl groups of PACMO for weakened lithium bonds. In addition, **Figure S10** exhibits that the TFSI⁻ peak of PAV shifts more significantly than that of PAE, further confirming that the TFSI⁻ of PIL is more involved on the coordination with Li⁺. Thereby, the lithium bonds are weakened with PIL by both the hydrogen bonds and cocrordination effect, resulting in a lower Li⁺ transfer barrier and much higher Li⁺ migration behavior.

The LF-NMR spectra further confirm the interaction evolution after copolymerizing [VEIM][TFSI]. The LF-NMR spectra of the electrolytes without LiFSI are shown in **Figure S11**, and the peak positions of the two gels are similar, suggesting the similar hydrogen bonds strength. Nevertheless, as exhibited in **Figure 3e**, the T_2 presents an obvious decrease in PAEV as compared with that in PAE. This indicates that the PIL not only participates in changing the ionic environment, but also enhances the compatibility of the [EMIM][TFSI] in PAEV, providing a uniform solvent environment for Li⁺ diffusion. DSC curves of PAE and PAEV electrolytes are compared in **Figure 3f** in the range between -80 and 120 °C. A weak exothermic peak can be observed in the PAE electrolyte, which can be ascribed to the crystallization of a small amount of free [EMIM][TFSI] in the PAE electrolyte. In contrast, no peaks can be observed in PAEV in the same temperature range, illustrating that the [EMIM][TFSI] is uniformly dispersed in PAEV with no crystallization, which can be benefiting to the polymer chains mobility and Li⁺ migration.

Furthermore, temperature-variable FTIR spectroscopy was employed to study the internal variations of $\nu(\text{C}=\text{O}\cdots\text{H})$ (hydrogen bonded carbonyl) and $\nu(\text{C}=\text{O}\cdots\text{Li}^+)$ (lithium bonded carbonyl) bands as the temperature increases. In **Figure S12**, the bands related to carbonyl groups render significant shift both for PAE and PAEV with the temperature increases from 30 to 150 °C. 2DCOS analysis was further carried out from the temperature-variable FTIR spectra of PAEV to reveal the specific molecular interactions in the electrolyte, as shown in **Figure 3g** and h. Based on Noda's rule, the change sequence of different species under external perturbation could be distinguished.^{35,36} Herein, according to the sign of the 2DCOS synchronous and asynchronous spectra (**Table S2**), the responsive order of carbonyl groups in

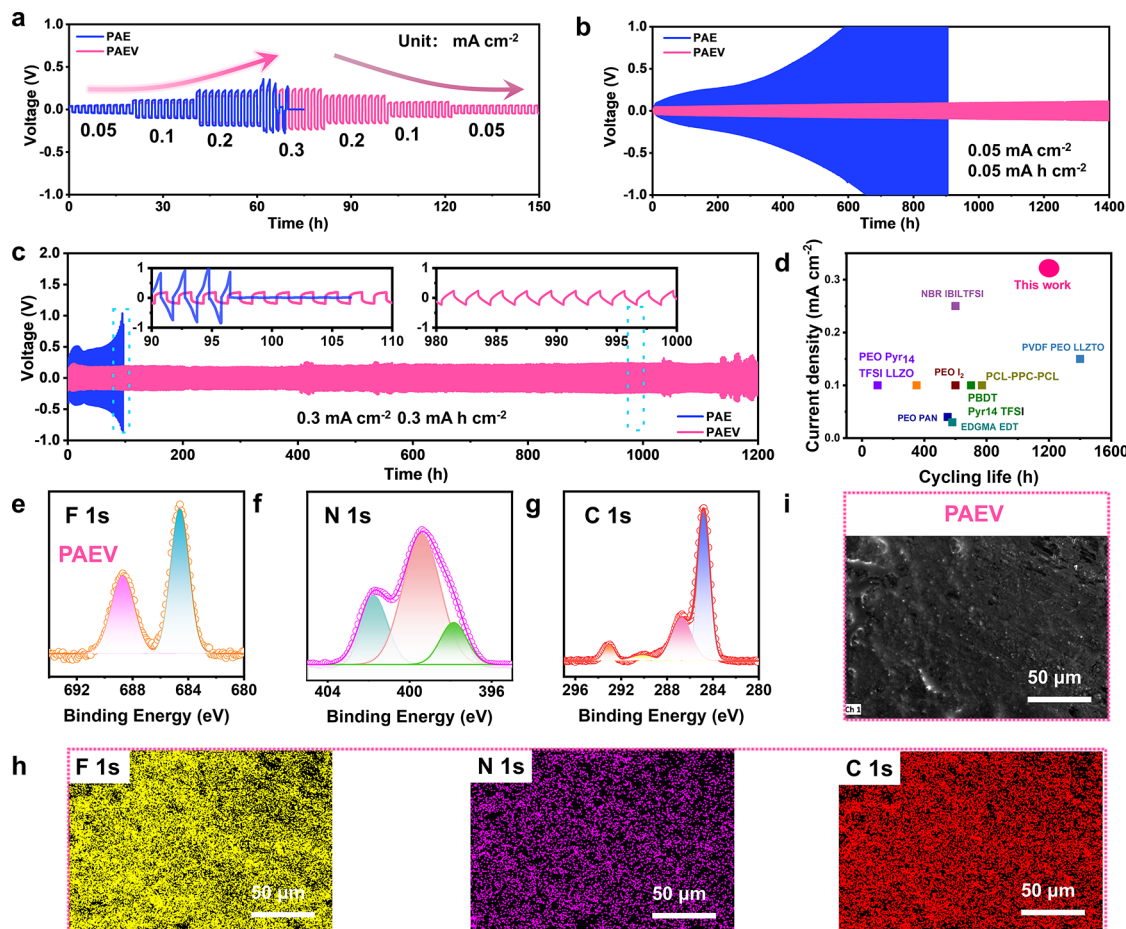


Figure 4. Dendrites' inhibition performances of the symmetrical lithium battery with different electrolyte. (a) Voltage profiles of the plating/stripping performance for the symmetrical batteries at different current density. Long-term cycling performance of the symmetrical batteries at a current density of (b) 0.05 mA cm^{-2} and (c) 0.3 mA cm^{-2} . (d) The dendrite inhibition performance of the PAEV electrolyte compared with recently reported literatures. XPS spectra of the lithium surface after cycling with PAEV for (e) F 1s, (f) N 1s, (g) C 1s. The (h) SEM image and (i) corresponding EDS results of the lithium anodes after cycling with PAEV for 100 h under the current density of 0.3 mA cm^{-2} .

different states upon heating can be determined as $1650 \rightarrow 1638 \rightarrow 1618 \text{ cm}^{-1}$, that is, $\text{C}=\text{O}$ in dipole–dipole interaction $\rightarrow \text{C}=\text{O}$ in hydrogen bonding $\rightarrow \text{C}=\text{O}$ in lithium bonding. On the one hand, the $\text{C}=\text{O}$ groups participated in different molecular interactions have been directly recognized.^{37,38} On the other hand, this order indicates a thermal sensitivity order of dipole–dipole interaction $>$ hydrogen bonding $>$ lithium bonding regarding to carbonyl groups, suggesting an interaction strength of lithium bonding $>$ hydrogen bonding $>$ dipole–dipole interaction (weak interaction holds a higher thermal sensitivity).

Density functional theory (DFT) is then conducted to further illustrate the interaction between Li, ACMO, [EMIM]-[TFSI] and [VEIM][TFSI]. As depicted in Figure 3i, the binding energy of [EMIM] [TFSI] to ACMO-co-[VEIM]-[TFSI] is higher than that of [EMIM] [TFSI] to ACMO, indicating the much higher interaction between the ionic liquid and the polymer with PIL. The binding energy of Li^+ and ACMO decreases with the addition of [EMIM][TFSI], due to the hydrogen bonds of [EMIM][TFSI] and ACMO. After copolymerizing with [VEIM][TFSI], the binding energy further reduces, which is ascribed to the cocomordination effect. This lower binding energy indicates that the lithium bonds are effectively weakened for rapid Li^+ migration.

In view of the cross-linking role of Li^+ , as predicted, the mechanical strength of electrolyte is reduced after the weakening of lithium bonds, as shown in Figure 3j. The reduced material rigidity is beneficial to improving the interfacial contact performance between electrolyte and electrode, facilitating to increase the ionic conductivity and Li/Li^+ transference.³⁹ The effect of PIL on the ionic conductivity is then demonstrated. As shown in Figure S13, with the increase of PIL, the ionic conductivity increased, due to the weakening of the lithium bonds. The ionic conductivity then decreases after the molar ratio of ACMO:[VEIM][TFSI] is lower than 4:1, possibly due to that the exceed amounts of PIL would provide strong electrostatic interaction with Li^+ , thus impeding their transport.²⁸ In addition, abundant PIL could increase the crystallinity of the electrolyte, creating crystalline regions which are not conductive for Li^+ .⁴⁰ The effect of different amounts of [EMIM][TFSI] on lithium bonds' construction was examined by FTIR spectroscopy (Figure S14a), which shows barely peak variations in this ratio range. However, the [EMIM][TFSI] can act as the plasticizer which regulates the mechanical properties and ionic conductivity of polymer electrolyte (SPE), as shown in Figure S14b and c. After comprehensive selection, the optimized content of [EMIM][TFSI] was fixed at 58 wt %.

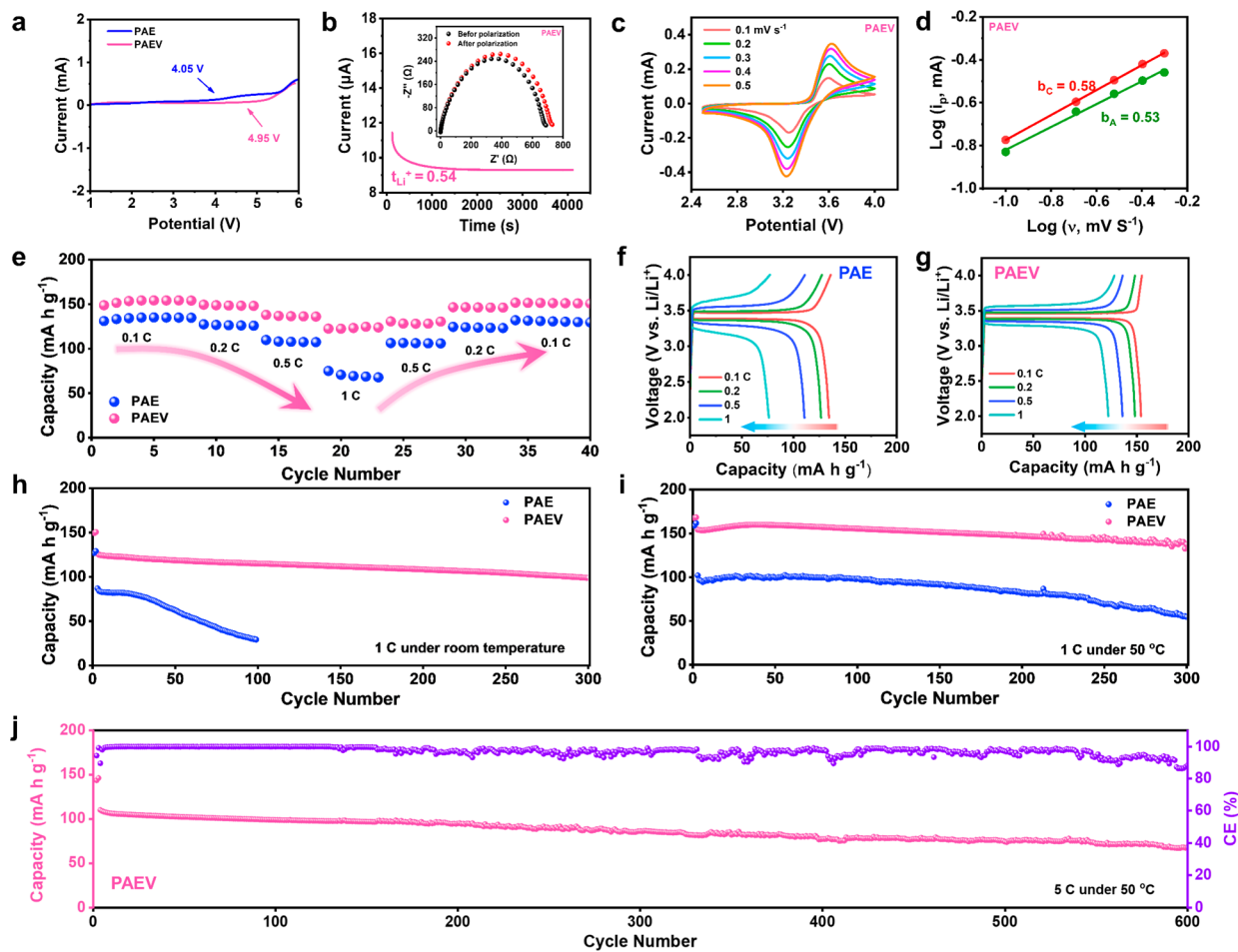


Figure 5. Electrochemical properties of the batteries with different electrolyte. (a) Linear sweep voltammogram (LSV) curves of PAEV and PAE. (b) The chronoamperometry profiles of symmetrical lithium batteries for PAEV with the applying DC voltage of 10 mV, the insets show the Nyquist impedance spectra of the battery before and after polarization. (c) CV curves of Li/LFP battery with PAEV at various sweep speeds. (d) The linear fitting plots of $\log(i_p)$ versus $\log(v)$. (e) Rate performance of Li/LFP cells with different electrolyte at room temperature and the corresponding charge/discharge profiles of (f) PAE and (g) PAEV. Cycling performance of Li/PAEV/LFP and Li/PAE/LFP at (h) room temperature and (i) 50 °C. (j) Long-term cycling properties of the Li/PAEV/LFP battery under 5 °C at 50 °C.

For clarity, the molecular interactions and the Li^+ transport mechanism in the electrolyte is summarized in Figure 3k. In PAE, Li^+ tends to bind with polymer chains rather than [EMIM][TFSI], leading to the aggregation of free [EMIM]-[TFSI] in the electrolyte. As a consequence, the Li^+ transports slowly on polymer chains which significantly limits the overall transport rate.^{41–43} In PAEV electrolytes, with the introduction of PIL, the hydrogen bonds between IL/PIL and PACMO are enhanced, enabling the ionic liquids uniformly distributed in the electrolyte, which provides a transport channel for Li^+ fast transfer.^{21,44} In addition, the cocrordination of PIL and Li^+ can further improve the Li^+ migration and weaken the Li bonds, resulting in faster transport kinetics.

Electrochemical Performance. The lithium dendrite formation behavior will seriously impede the lithium batteries practical applications. The symmetrical lithium batteries with different polymer electrolytes were assembled and the lithium dendrite inhibition performance were evaluated by plating/stripping at different current densities. In Figure 4a, with the current density increased from 0.05 to 0.3 mA cm^{-2} , the battery with PAE becomes short circuit, whereas the battery with PAEV can keep stable and return back to 0.05 mA cm^{-2} . Moreover, the voltage polarization of the battery with PAEV is

always lower than PAE at all the current densities, demonstrating the optimized Li^+ transport in PAEV electrolyte due to the lithium bonds regulation. For long cycling performance, at the current density of 0.05 mA cm^{-2} , the battery with PAEV can keep stable for more than 1400 h (Figure 4b). On the contrary, the voltage polarization of the battery with PAE keeps on increasing during cycling, due to the generation of dead Li and Li dendrites, which resist the Li^+ transport and Li/Li^+ transference. Even at the higher current density of 0.3 mA cm^{-2} , the battery with PAEV can still provide a stable cycling for 1200 h as depicted in Figure 4c, which is much longer than PAE (around 100 h before short circuit). This excellent dendrite inhibition performance has already suppressed many recently reported polymer batteries,^{45–51} ascribing to the optimized Li^+ transport in the PAEV electrolyte, and the great mechanical properties which improve the interfacial compatibility between PAEV and Li anode (Figure 4d). SEM images of the lithium anode before and after cycling for 100 h under the current density of 0.3 mA cm^{-2} were characterized and shown in Figure S15; the anode with PAEV after cycling is still flat and dendrite free, which is consistent with the symmetrical lithium battery performance. By contrast, the lithium anode with PAE after 100 h cycling

provides a rough surface with dead lithium and dendrite formation, originated to the low Li^+ transport, uneven Li/Li^+ transference and inferior interfacial contact. The X-ray photoelectron spectroscopy (XPS) was then implemented to characterize the SEI composition evolution during cycling. As depicted in Figure 4e-g and Figure S16, only after 20 cycles do the peaks at 685 eV for LiF and 397 eV for Li_3N increase significantly in PAEV comparing to PAE, demonstrating that with the regulated lithium bonds and ionic liquid distribution, the inorganic contents are much easily formed in the SEI layers for faster Li^+ transport, uniform lithium deposition, and better dendrite inhibition performance. EDS results for the Li surface after cycling further illustrate the uniform distribution of LiF and Li_3N of the battery with PAEV (Figure 4h, i).

Linear sweep voltammetry (LSV) was then conducted to test the electrochemical stability window of the electrolyte. As Figure 5a displays, the PAEV can remain stable up to 4.95 V, much higher than PAE of 4.05 V, which owns the potential for high voltage batteries. The Li^+ transference number (t_{Li}^{+}) is then measured and depicted in Figure 5b and S17. The t_{Li}^{+} of the PAEV can be as high as 0.54, which is significantly higher than PAE (0.22) and reported PEO based polymer state electrolyte (around 0.19 ± 0.02).⁵² This can be attributed to the hydrogen bonds formation between [VEIM][TFSI] and carbonyl groups, and the cocomoordination behavior occurs among PIL, TFSI⁻ and Li^+ , which effectively weaken the lithium bonds between Li^+ and carbonyl group, and avoid the direct interaction between polymer backbone and Li^+ to further facilitate the Li^+ transport in PAEV electrolyte. Moreover, the TFSI⁻ anion motion in PAEV is more confined than PAE due to the cocomoordination, resulting in the much higher Li^+ transference number for PAEV.^{34,53}

In order to further confirm the ion transport and electrochemical kinetics of the electrolytes, the CV curves for Li/LFP batteries were characterized and the diffusion coefficient of Li^+ (D_{Li}^+) was calculated (Figure 5c, Figure S18 and Table S3). As shown, the Li^+ diffusion coefficient in PAEV electrolyte is much larger than that of PAE, due to the improved Li^+ transport route in PAEV electrolyte. The PAEV 7:1 electrolyte can only render the lowest Li^+ diffusion coefficient with the highest coordination number of Li^+ . As for PAEV of 1.5:1, ionic complexes formed by the excess lithium salts, and the Li^+ transport is also hindered. The b value for the capacity contribution was also calculated.⁵⁴ As Figure 5d shows, the b values of the anodic peak and cathodic peak are 0.58 and 0.53, respectively, further verifying that the ion migration in PAEV is faster. The GITT result is provided in Figure S19. With PAEV, the battery delivers a stable charge/discharge behavior with small polarization (0.1 V), benefiting from the faster Li^+ migration rate in PAEV.⁵⁵

The cycling performance of Li/PAEV/LFP batteries was then employed and characterized at both room temperature and 50 °C. As shown in Figure 5e, the battery with PAEV can provide a high reversible capacity of 154, 148, 136, and 124 mA h g⁻¹ at the current density of 0.1, 0.2, 0.5, and 1 C, which are all higher than PAE of 134, 123, 107, and 74 mA h g⁻¹, benefiting from the high Li^+ diffusion coefficient and ionic conductivities of PAEV electrolyte. The corresponding charge/discharge curves are shown in Figure 5f and 5g, and the Li/PAEV/LFP battery exhibits the more stable voltage plateau at all current densities. For the long-term cycling performance at room temperature (Figure 5h), the battery with PAEV can deliver a high capacity of 100 mA h g⁻¹ after 300 cycles at 1 C,

and the PAE battery can only remain stable for less than 25 cycles before sharply decreasing, due to the low Li^+ conductivity and dendrite formation. When operated at 50 °C, as depicted in Figure 5i, the battery with PAEV can deliver a high initial capacity of 152 mA h g⁻¹ at 1 C, and a capacity retention for more than 92% after 300 cycles, which are both higher than PAE battery due to the lithium bonds weakening and ionic conductivity increasing. Even at a higher current density of 5 C, the battery with PAEV can still exhibit a stable capability of 70 mA h g⁻¹ after 600 cycles (Figure 5j). The prototype pouch cell was finally assembled and tested, which can simply power the hygrometer, and keep the voltage stability under bending, folding and shearing, demonstrating good practical application potentials of the PAEV electrolyte (Figure S20).

CONCLUSIONS

In conclusion, a polymer electrolyte PAEV with regulated lithium bonds and hydrogen bonds is successfully engineered for lithium batteries. The lithium bonds formed between Li^+ and the carbonyl groups in PACMO chains, can be modulated by adjusting the coordination number of Li^+ , resulting in good mechanical property and high ionic conductivity of the electrolyte. The modified mechanical property can confer the electrolyte with excellent interfacial adaptivity to the electrode, which facilitated the Li/Li^+ transference, lithium nucleation, and Li^+ transport. Furthermore, copolymerizing [VEIM]-[TFSI] in the network can form hydrogen bonds with PACMO chains to weaken the lithium transfer barrier in the electrolyte and exhibit cocomoordination behavior to increase the Li^+ diffusion coefficients. Therefore, the resulting PAEV electrolyte enables the symmetrical Li battery with high reversible plating/stripping performance for more than 1200 h at the high current density of 0.3 mA cm⁻² at room temperature. The LiFePO₄ battery with PAEV can cycle stably with high capacity both at room temperature and 50 °C. This work provides an observation of the regulation of lithium bonds in the polymer gel and demonstrates a facile strategy on synchronously manipulating the mechanical and electrochemical properties for high performance polymer state lithium batteries.

EXPERIMENTAL SECTION

Materials. The ACMO was purchased from Adamas. [EMIM][TFSI] was obtained from Rhawn Chemical. Li bis-(trifluoromethylsulfonyl)imide (LiTFSI), LiFSI, bromoethane, ethyl acetate and vinylimidazole were purchased from Aladdin; 2-hydroxy-4'-(2-hydroxyethoxy)-2-methylpropiophenone (Irgacure 2959) was purchased from Sigma-Aldrich.

Preparation of [VEIM][TFSI] Monomer. The bromoethane (12 g) and vinylimidazole (9.4 g) were mixed in the ethyl acetate solution (10 g) and stirred for 48 h at room temperature. The resulting mixture was washed with ethyl acetate and dried by a vacuum oven to obtain the 1-vinyl-3-ethyl imidazolium ([VEIM][Br]) particles. Afterward, the [VEIM][Br] and LiTFSI in the same molar ratio were dissolved in deionized water and stirred for 12 h to achieve an oily liquid. The oily liquid was then washed with deionized water for three times and dried for 24 h in a vacuum oven to obtain the [VEIM][TFSI].

Preparation of the PAEV and PAE Electrolyte. For the preparation of PAEV, typically, a mixture of ACMO (0.4 g), [VEIM][TFSI] (0.27 g), [EMIM][TFSI] (1 g), LiFSI (0.14 g), and Irgacure 2959 (UV curing initiator, 2 wt % of the total monomer) were stirred in a vial for 12 h and vacuum treated before polymerization. (The molar ratio of ACMO to [VEIM][TFSI] is

4:1, and the content of [EMIM][TFSI] is 58% of the total mass for PAEV.) Afterward, the mixture was poured into a glass mold and polymerized with UV lamp equipment (wavelength: 365 nm, power: 100 W) for 20 min to form the PAEV electrolyte. The PAEV electrolytes with different mechanical properties and ionic conductivities were synthesized by varying the ratio of ACMO and LiFSI. The electrolyte without [VEIM][TFSI] (PAE for short) was prepared using the same method in the absence of [VEIM][TFSI].

Characterization. The Fourier Transform infrared (FTIR) spectroscopy, nuclear magnetic resonance (NMR), and low-field nuclear magnetic resonance (LF NMR) were collected by Nicolet iS50 FTIR, Bruker Avance-400, and Newmag VTMR20-010V-I, respectively, for the interaction characterizations of the polymer electrolyte. The scanning electron microscopy (SEM, Hitachi SU8230) was employed for the morphology inspection of the polymer electrolyte and Li metal. Thermo stability was measured by the thermogravimetric analysis (TGA, TA Q550) under N_2 atmosphere with a heating rate of 10 °C/min. The mechanical test was performed by the tensile machine (UTM2103, Shenzhen suns technology CO., Ltd.).

The ionic conductivity (σ) of the polymer electrolyte was analyzed by electrochemical impedance spectroscopy (EIS) on an Autolab (Metrohm) ranging from 1 MHz to 0.01 Hz. The results were calculated by the following equation:

$$\sigma = \frac{L}{RS} \quad (1)$$

where L represents the thickness of polymer electrolyte, R is the bulk resistance and S is the area of the electrolyte.

The Arrhenius equation was employed to fit the ionic conductivity of polymer electrolyte in different temperature:

$$\sigma = A \exp\left(-\frac{E_a}{k_B T}\right) \quad (2)$$

where A is exponential factor, k_B is the Boltzmann constant, T is the Kelvin temperature, σ is the ionic conductivity and E_a is the activation energy.

The transference number of Li^+ (t_{Li^+}) was characterized by chronoamperometry and calculated by the following equation:

$$t_{Li^+} = \frac{I_{SS}(\Delta V - I_0 R_0)}{I_0(\Delta V - I_{SS} R_{SS})} \quad (3)$$

The ΔV stands for the polarization potential difference (10 mV), I_0 and I_{SS} represent the initial and steady-state currents of chronoamperometry, R_0 and R_{SS} are the initial and steady-state interfacial resistance before and after polarization.

The Li coordination numbers (χ) of bound TFSI⁻ in this system was calculated by the following equation:

$$\chi = \frac{A_{F1}}{A_{F1} + A_{F2}} \quad (4)$$

where A_{F1} and A_{F2} correspond to the integrated area of the F1 and F2 band, respectively.

The diffusion coefficient of Li^+ (D_{Li^+}) was calculated by the Randles–Sevcik equation:

$$i_p = 2.69 \times 10^5 n^{3/2} AD_{Li}^{1/2} C_{Li} v^{1/2} \quad (5)$$

where i_p is the peak current, n is the number of transferred electrons, A is the electrode area, D_{Li} is the diffusion coefficient of Li^+ , C_{Li} is the concentration of Li^+ and v is the sweep speed.

The coordination numbers (N) of carbonyls with Li^+ was obtained by evaluating the area ratio of coordinated carbonyl to the total area of carbonyl peaks. The calculation methods are described in the previous literatures with the following equation:^{56,57}

$$f_{CO} = \frac{A_{CO}}{A_{CO} + A_{UC}} \quad (6)$$

$$N = \frac{A_{CO}}{A_{CO} + A_{UC}} \times \frac{n_{C=O}}{n_{salt}} \quad (6)$$

where f_{CO} is the coordination percentage of $C=O$ to Li^+ , A_{CO} is the area of coordinated $C=O$, A_{UC} is the area of uncoordinated $C=O$, N is the coordination number, $n_{C=O}$ is the molar of ACMO and n_{salt} is the molar of salt.

Density Functional Theory (DFT) Calculations. Density functional theory (DFT) was performed to calculate the interactions between Li^+ , ACMO, [EMIM][TFSI] and [VEIM][TFSI] with the Gaussian 16 package. The geometry optimization was carried out by B3LYP/6-31G(d), including the atom-pairwise dispersion (DFT-D3) correction with Becke–Johnson (BJ) damping. To obtain a more accurate energy, single-point calculations of the optimized structures were carried out at B3LYP/def2-TZVP including the DFT-D3(BJ) correction. The Basis Set Superposition Error (BSSE) was taken into account in calculating the binding energy by counterpoise method proposed by Boys and Bernardi. The binding energy ($E(AB)$ Binding) was calculated as follows:

$$E(AB)_{\text{Binding}} = E(AB) - E(A) - E(B) + \text{BSSE} \quad (7)$$

where $E(AB)$, $E(A)$, and $E(B)$ stand for the single-point energy of complex AB, component A, component B, respectively.

Temperature-Variable FTIR Spectra Test. A film of the electrolyte was polymerized with a thickness of 100 μm , and then sealed by two zinc selenide sheets in the glovebox. The heating rate was 2 °C/min, and the FTIR curves were collected every minute.

ASSOCIATED CONTENT

Supporting Information

The Supporting Information is available free of charge at <https://pubs.acs.org/doi/10.1021/acsnano.2c11734>.

FTIR spectra of the [VEIM][TFSI], [EMIM][TFSI], PAEV, PACMO, PACMO/[EMIM][TFSI] and PAE; the fitted FTIR spectra of the electrolyte; coordination fraction of $C=O$ groups with Li^+ ; Raman spectra of electrolytes; LF-NMR spectra of PAE, PAE without LiFSI and pure [EMIM][TFSI]; Digital images of PAE and PAEV; FTIR spectra of electrolytes; LF-NMR curves of the PAE and PAEV without LiFSI; temperature-variable FTIR spectra; ionic conductivities; surface and cross-sectional SEM images of the lithium anodes; XPS spectra, SEM image and the corresponding EDS results of the lithium surface after cycling with PAE; chronoamperometry profile; CV curves of Li/LFP battery with PAE and PAEV; GITT profiles of the Li/LFP battery with PAEV; schematic illustrations of the Li/PAEV/LFP pouch cell (PDF)

A movie demonstrating the excellent nonflammability of PAEV (MP4)

AUTHOR INFORMATION

Corresponding Authors

Peiyi Wu – State Key Laboratory for Modification of Chemical Fibers and Polymer Materials, College of Chemistry and Chemical Engineering, Key Laboratory of Science & Technology of Eco-Textile, Ministry of Education, and Center for Advanced Low-Dimension Materials, Donghua University, Shanghai 201620, China; orcid.org/0000-0001-7235-210X; Email: wupeiyi@dhu.edu.cn

Yucong Jiao – State Key Laboratory for Modification of Chemical Fibers and Polymer Materials, College of Chemistry and Chemical Engineering, Donghua University, Shanghai 201620, China; Email: yucong.jiao@dhu.edu.cn

Authors

Zhilong Tian – State Key Laboratory for Modification of Chemical Fibers and Polymer Materials, College of Chemistry and Chemical Engineering, Donghua University, Shanghai 201620, China

Lei Hou – State Key Laboratory for Modification of Chemical Fibers and Polymer Materials, College of Chemistry and Chemical Engineering, Donghua University, Shanghai 201620, China

Doudou Feng – State Key Laboratory for Modification of Chemical Fibers and Polymer Materials, College of Chemistry and Chemical Engineering, Donghua University, Shanghai 201620, China

Complete contact information is available at:
<https://pubs.acs.org/10.1021/acsnano.2c11734>

Author Contributions

#Z.T. and L.H. contributed equally to this work. Y.J., and P.W. conceived and directed the project. Z.T. carried out all the experiments. L.H provided help on the characterization and analysis of the experiment results. D.F. provided help on the manuscript preparation and Figures drawing. All authors discussed the results and commented on the manuscript.

Notes

The authors declare no competing financial interest.

ACKNOWLEDGMENTS

The authors appreciate the supports from National Science Foundation of China (NSFC) (Nos. 51973035, 21991123, 51903041). They also thank Dr. Tianyu Li from Dalian Institute of Chemical Physics, Chinese Academy of Sciences for the DFT characterization.

REFERENCES

- (1) Lin, D.; Liu, Y.; Cui, Y. Reviving the Lithium Metal Anode for High-Energy Batteries. *Nat. Nanotech.* **2017**, *12*, 194–206.
- (2) Zhamu, A.; Chen, G.; Liu, C.; Neff, D.; Fang, Q.; Yu, Z.; Xiong, W.; Wang, Y.; Wang, X.; Jang, B. Z. Reviving Rechargeable Lithium Metal Batteries: Enabling Next-Generation High-Energy and High-Power Cells. *Energy Environ. Sci.* **2012**, *5*, 5701–5707.
- (3) Guo, Y.; Li, H.; Zhai, T. Reviving Lithium-Metal Anodes for Next-Generation High-Energy Batteries. *Adv. Mater.* **2017**, *29*, 1700007.
- (4) Lopez, J.; Pei, A.; Oh, J. Y.; Wang, G. N.; Cui, Y.; Bao, Z. Effects of Polymer Coatings on Electrodeposited Lithium Metal. *J. Am. Chem. Soc.* **2018**, *140*, 11735–11744.
- (5) Lopez, J.; Mackanic, D. G.; Cui, Y.; Bao, Z. Designing Polymers for Advanced Battery Chemistries. *Nat. Rev. Mater.* **2019**, *4*, 312–330.
- (6) An, S. Y.; Jeong, I. C.; Won, M.-S.; Jeong, E. D.; Shim, Y.-B. Effect of Additives in PEO/PAA/PMAA Composite Solid Polymer Electrolytes on the Ionic Conductivity and Li Ion Battery Performance. *J. Appl. Electrochem.* **2009**, *39*, 1573–1578.
- (7) Fan, L. Z.; Hu, Y. S.; Bhattacharyya, A. J.; Maier, J. Succinonitrile As a Versatile Additive for Polymer Electrolytes. *Adv. Funct. Mater.* **2007**, *17*, 2800–2807.
- (8) Li, J.; Lin, Y.; Yao, H.; Yuan, C.; Liu, J. Tuning Thin-Film Electrolyte for Lithium Battery by Grafting Cyclic Carbonate and Combed Poly(Ethylene Oxide) on Polysiloxane. *ChemSusChem* **2014**, *7*, 1901–1908.
- (9) Zhang, Z. C.; Sherlock, D.; West, R.; West, R.; Amine, K.; Lyons, L. J. Cross-Linked Network Polymer Electrolytes Based on a Polysiloxane Backbone with Oligo(Oxyethylene) Side Chains: Synthesis and Conductivity. *Macromol.* **2003**, *36*, 9176–9180.
- (10) Xue, Z.; He, D.; Xie, X. Poly(Ethylene Oxide)-Based Electrolytes for Lithium-Ion Batteries. *J. Mater. Chem. A* **2015**, *3*, 19218–19253.
- (11) Shim, J.; Kim, D.-G.; Kim, H. J.; Lee, J. H.; Baik, J.-H.; Lee, J.-C. Novel Composite Polymer Electrolytes Containing Poly(Ethylene Glycol)-Grafted Graphene Oxide for All-Solid-State Lithium-Ion Battery Applications. *J. Mater. Chem. A* **2014**, *2*, 13873–13883.
- (12) Tominaga, Y.; Yamazaki, K. Fast Li-Ion Conduction In Poly(Ethylene Carbonate)-Based Electrolytes and Composites Filled with TiO₂ Nanoparticles. *Chem. Commun.* **2014**, *50*, 4448–4450.
- (13) Wang, H.; Sheng, L.; Yasin, G.; Wang, L.; Xu, H.; He, X. Reviewing the Current Status and Development of Polymer Electrolytes for Solid-State Lithium Batteries. *Energy Storage Mater.* **2020**, *33*, 188–215.
- (14) Wang, Y.; Zanelotti, C. J.; Wang, X.; Kerr, R.; Jin, L.; Kan, W. H.; Dingemans, T. J.; Forsyth, M.; Madsen, L. A. Solid-State Rigid-Rod Polymer Composite Electrolytes with Nanocrystalline Lithium Ion Pathways. *Nat. Mater.* **2021**, *20*, 1255–1263.
- (15) Wang, X.; Chen, F.; Girard, G. M. A.; Zhu, H.; MacFarlane, D. R.; Mecerreyes, D.; Armand, M.; Howlett, P. C.; Forsyth, M. Poly(Ionic Liquid)s-in-Salt Electrolytes with Co-Coordination-Assisted Lithium-Ion Transport for Safe Batteries. *Joule* **2019**, *3*, 2687–2702.
- (16) Sannigrahi, A. B.; Kar, T.; Niyogi, B. G.; Hobza, P.; Schleyer, P. V. The Lithium Bond Reexamined. *Chem. Rev.* **1990**, *90*, 1061–1076.
- (17) Ritchie, J. P.; Bachrach, S. M. Bond Paths and Bond Properties of Carbon-Lithium Bonds. *J. Am. Chem. Soc.* **1987**, *109*, 5909–5916.
- (18) Vila, A.; Vila, E.; Mosquera, R. A. Topological Characterisation of Intermolecular Lithium Bonding. *Chem. Phys.* **2006**, *326*, 401–408.
- (19) Chen, X.; Bai, Y. K.; Zhao, C. Z.; Shen, X.; Zhang, Q. Lithium Bonds in Lithium Batteries. *Angew. Chem. Int. Ed.* **2020**, *59*, 11192–11195.
- (20) Yiming, B.; Han, Y.; Han, Z.; Zhang, X.; Li, Y.; Lian, W.; Zhang, M.; Yin, J.; Sun, T.; Wu, Z.; Li, T.; Fu, J.; Jia, Z.; Qu, S. A Mechanically Robust and Versatile Liquid-Free Ionic Conductive Elastomer. *Adv. Mater.* **2021**, *33*, 2006111.
- (21) Cai, X.; Ye, B.; Ding, J.; Chi, Z.; Sun, L.; Saha, P.; Wang, G. Dual Li-Ion Migration Channels in an Ester-Rich Copolymer/Ionic Liquid Quasi-Solid-State Electrolyte for High-Performance Li–S Batteries. *J. Mater. Chem. A* **2021**, *9*, 2459–2469.
- (22) Chai, J.; Liu, Z.; Ma, J.; Wang, J.; Liu, X.; Liu, H.; Zhang, J.; Cui, G.; Chen, L. *In Situ* Generation of Poly (Vinylene Carbonate) Based Solid Electrolyte with Interfacial Stability for LiCoO₂ Lithium Batteries. *Adv. Sci.* **2017**, *4*, 1600377.
- (23) Tominaga, Y.; Yamazaki, K.; Nanthana, V. Effect of Anions on Lithium Ion Conduction in Poly(Ethylene Carbonate)-Based Polymer Electrolytes. *J. Electrochem. Soc.* **2015**, *162*, A3133–A3136.
- (24) Wang, L.; Wang, Y.; Yang, S.; Tao, X.; Zi, Y.; Daoud, W. A. Solvent-Free Adhesive Ionic Elastomer for Multifunctional Stretchable Electronics. *Nano Energy* **2022**, *91*, 106611.
- (25) Chen, F.; Guo, C.; Zhou, H.; Shahzad, M. W.; Liu, T. X.; Oleksandr, S.; Sun, J.; Dai, S.; Xu, B. B. Supramolecular Network Structured Gel Polymer Electrolyte with High Ionic Conductivity for Lithium Metal Batteries. *Small* **2022**, *18*, 2106352.
- (26) Cordier, F.; Rogowski, M.; Grzesiek, S.; Bax, A. Observation of Through-Hydrogen-Bond ²HJHC' in a Perdeuterated Protein. *J. Magn. Reson.* **1999**, *140*, 510–512.
- (27) Mackanic, D. G.; Michaels, W.; Lee, M.; Feng, D.; Lopez, J.; Qin, J.; Cui, Y.; Bao, Z. Crosslinked Poly(Tetrahydrofuran) as a Loosely Coordinating Polymer Electrolyte. *Adv. Energy Mater.* **2018**, *8*, 1800703.
- (28) Cao, Z.; Liu, H.; Jiang, L. Transparent, Mechanically Robust, and Ultrastable Ionogels Enabled by Hydrogen Bonding Between Elastomers and Ionic Liquids. *Mater. Horiz.* **2020**, *7*, 912–918.
- (29) Hardwick, L. J.; Holzapfel, M.; Wokaun, A.; Novák, P. Raman Study of Lithium Coordination in EMI-TFSI Additive Systems as Lithium-Ion Battery Ionic Liquid Electrolytes. *J. Raman Spectrosc.* **2007**, *38*, 110–112.

- (30) Duluard, S.; Grondin, J.; Bruneel, J.-L.; Pianet, I.; Grélard, A.; Campet, G.; Delville, M.-H.; Lassègues, J.-C. Lithium Solvation and Diffusion in the 1-Butyl-3-Methylimidazolium Bis-(Trifluoromethanesulfonyl)Imide Ionic Liquid. *J. Raman Spectrosc.* **2008**, *39*, 627–632.
- (31) Zhao, G.; Sun, X.; Zhang, L.; Chen, X.; Mao, Y.; Sun, K. A Self-Supported Metal-Organic Framework Derived Co_3O_4 Film Prepared by an *In-Situ* Electrochemically Assistant Process as Li Ion Battery Anodes. *J. Power Sources* **2018**, *389*, 8–12.
- (32) Yui, T.; Shiiba, H.; Tsutsumi, Y.; Hayashi, S.; Miyata, T.; Hirata, F. Systematic Docking Study of the Carbohydrate Binding Module Protein of Cel7A with the Cellulose I α Crystal Model. *J. Phys. Chem. C* **2010**, *114*, 49–58.
- (33) Miller, T. F.; Wang, Z. G.; Coates, G. W.; Balsara, N. P. Designing Polymer Electrolytes for Safe and High Capacity Rechargeable Lithium Batteries. *Acc. Chem. Res.* **2017**, *50*, 590–593.
- (34) Pablos, J. L.; García, N.; Garrido, L.; Catalina, F.; Corrales, T.; Tiemblo, P. Polycationic Scaffolds for Li-Ion Anion Exchange Transport in Ion Gel Polyelectrolytes. *J. Mater. Chem. A* **2018**, *6*, 11215–11225.
- (35) Sun, S. T.; Wu, P. Y. Spectral Insights into Microdynamics of Thermoresponsive Polymers from the Perspective of Two-Dimensional Correlation Spectroscopy. *Chin. J. Polym. Sci.* **2017**, *35*, 700–712.
- (36) Noda, I. Generalized Two-Dimensional Correlation Method Applicable to Infrared, Raman, and Other Types of Spectroscopy. *Appl. Spectrosc.* **1993**, *47*, 1329.
- (37) Gong, K.; Hou, L.; Wu, P. Hydrogen-Bonding Affords Sustainable Plastics with Ultrahigh Robustness and Water-Assisted Arbitrarily Shape Engineering. *Adv. Mater.* **2022**, *34*, 2201065.
- (38) Zhang, W.; Wu, B.; Sun, S.; Wu, P. Skin-Like Mechanoresponsive Self-Healing Ionic Elastomer From Supramolecular Zwitterionic Network. *Nat. Commun.* **2021**, *12*, 4082.
- (39) Han, X.; Gong, Y.; Fu, K. K.; He, X.; Hitz, G. T.; Dai, J.; Pearse, A.; Liu, B.; Wang, H.; Rubloff, G.; Mo, Y.; Thangadurai, V.; Wachsman, E. D.; Hu, L. Negating Interfacial Impedance in Garnet-Based Solid-State Li Metal Batteries. *Nat. Mater.* **2017**, *16*, 572–579.
- (40) Zhang, F.; Sun, Y.; Wang, Z.; Fu, D.; Li, J.; Hu, J.; Xu, J.; Wu, X. Highly Conductive Polymeric Ionic Liquid Electrolytes for Ambient-Temperature Solid-State Lithium Batteries. *ACS Appl. Mater. Interfaces* **2020**, *12*, 23774–23780.
- (41) Sun, H.; Zhu, G.; Zhu, Y.; Lin, M. C.; Chen, H.; Li, Y. Y.; Hung, W. H.; Zhou, B.; Wang, X.; Bai, Y.; Gu, M.; Huang, C. L.; Tai, H. C.; Xu, X.; Angell, M.; Shyue, J. J.; Dai, H. High-Safety and High-Energy-Density Lithium Metal Batteries in a Novel Ionic-Liquid Electrolyte. *Adv. Mater.* **2020**, *32*, 2001741.
- (42) Jafta, C. J.; Sun, X. G.; Lyu, H.; Chen, H.; Thapaliya, B. P.; Heller, W. T.; Cuneo, M. J.; Mayes, R. T.; Paranthaman, M. P.; Dai, S.; Bridges, C. A. Insight into the Solid Electrolyte Interphase Formation in Bis(Fluorosulfonyl)Imide Based Ionic Liquid Electrolytes. *Adv. Funct. Mater.* **2021**, *31*, 2008708.
- (43) Wei, X. Y.; Shriver, D. F. Highly Conductive Polymer Electrolytes Containing Rigid Polymers. *Chem. Mater.* **1998**, *10*, 2307–2308.
- (44) Liu, Z.; Zhou, W.; Wang, C.; Hu, W.; Chen, Z. Cotton Thread Modified with Ionic Liquid Copolymerized Polymer for Online In-Tube Solid-Phase Microextraction and HPLC Analysis of Non-steroidal Anti-Inflammatory Drugs. *J. Sep. Sci.* **2020**, *43*, 2827–2833.
- (45) Zhang, B.; Liu, Y.; Pan, X.; Liu, J.; Doyle-Davis, K.; Sun, L.; Liu, J.; Jiao, X.; Jie, J.; Xie, H.; Sun, X. Dendrite-Free Lithium Metal Solid Battery with a Novel Polyester Based Triblock Copolymer Solid-State Electrolyte. *Nano Energy* **2020**, *72*, 104690.
- (46) Lin, Y.; Wu, M.; Sun, J.; Zhang, L.; Jian, Q.; Zhao, T. A High-Capacity, Long-Cycling All-Solid-State Lithium Battery Enabled by Integrated Cathode/Ultrathin Solid Electrolyte. *Adv. Energy Mater.* **2021**, *11*, 2101612.
- (47) Yu, D.; Pan, X.; Bostwick, J. E.; Zanelotti, C. J.; Mu, L.; Colby, R. H.; Lin, F.; Madsen, L. A. Room Temperature to 150 °C Lithium Metal Batteries Enabled by a Rigid Molecular Ionic Composite Electrolyte. *Adv. Energy Mater.* **2021**, *11*, 2003559.
- (48) Shi, P.; Ma, J.; Huang, Y.; Fu, W.; Li, S.; Wang, S.; Zhang, D.; He, Y.-B.; Kang, F. A Thin and High-Strength Composite Polymer Solid-State Electrolyte with a Highly Efficient and Uniform Ion-Transport Network. *J. Mater. Chem. A* **2021**, *9*, 14344–14351.
- (49) Zhang, S.; Liang, T.; Wang, D.; Xu, Y.; Cui, Y.; Li, J.; Wang, X.; Xia, X.; Gu, C.; Tu, J. A Stretchable and Safe Polymer Electrolyte with a Protecting-Layer Strategy for Solid-State Lithium Metal Batteries. *Adv. Sci.* **2021**, *8*, 2003241.
- (50) Shi, Y.; Yang, N.; Niu, J.; Yang, S.; Wang, F. A Highly Durable Rubber-Derived Lithium-Conducting Elastomer for Lithium Metal Batteries. *Adv. Sci.* **2022**, *9*, 2200553.
- (51) Sheng, O.; Hu, H.; Liu, T.; Ju, Z.; Lu, G.; Liu, Y.; Nai, J.; Wang, Y.; Zhang, W.; Tao, X. Interfacial and Ionic Modulation of Poly(Ethylene Oxide) Electrolyte via Localized Iodization to Enable Dendrite-Free Lithium Metal Batteries. *Adv. Funct. Mater.* **2022**, *32*, 2111026.
- (52) Long, L.; Wang, S.; Xiao, M.; Meng, Y. Polymer Electrolytes for Lithium Polymer Batteries. *J. Mater. Chem. A* **2016**, *4*, 10038–10069.
- (53) Li, Z. H.; Xia, Q. L.; Liu, L. L.; Lei, G. T.; Xiao, Q. Z.; Gao, D. S.; Zhou, X. D. Effect of Zwitterionic Salt on the Electrochemical Properties of a Solid Polymer Electrolyte with High Temperature Stability for Lithium Ion Batteries. *Electrochim. Acta* **2010**, *56*, 804–809.
- (54) Wen, P.; Lu, P.; Shi, X.; Yao, Y.; Shi, H.; Liu, H.; Yu, Y.; Wu, Z. S. Photopolymerized Gel Electrolyte with Unprecedented Room-Temperature Ionic Conductivity for High-Energy-Density Solid-State Sodium Metal Batteries. *Adv. Energy Mater.* **2021**, *11*, 2002930.
- (55) Kim, D.-H.; Hwang, S.; Cho, J.-J.; Yu, S.; Kim, S.; Jeon, J.; Ahn, K. H.; Lee, C.; Song, H.-K.; Lee, H. Toward Fast Operation of Lithium Batteries: Ion Activity As the Factor To Determine the Concentration Polarization. *ACS Energy Lett.* **2019**, *4*, 1265–1270.
- (56) Chapman, N.; Borodin, O.; Yoon, T.; Nguyen, C. C.; Lucht, B. L. Spectroscopic and Density Functional Theory Characterization of Common Lithium Salt Solvates in Carbonate Electrolytes for Lithium Batteries. *J. Phys. Chem. C* **2017**, *121*, 2135–2148.
- (57) Seo, D. M.; Reininger, S.; Kutcher, M.; Redmond, K.; Euler, W. B.; Lucht, B. L. Role of Mixed Solvation and Ion Pairing in the Solution Structure of Lithium Ion Battery Electrolytes. *J. Phys. Chem. C* **2015**, *119*, 14038–14046.